Vol 14 No 5, May 2005
1009-1963/2005/14(05)/0935-07

Chinese Physics

© 2005 Chin. Phys. Soc.
and IOP Publishing Ltd

Imaging properties of coherent anti-Stokes Raman scattering microscope

Yuan Jing-He(袁景和)[a)b)†] Xiao Fan-Rong(肖繁荣)[a)],
Wang Gui-Ying(王桂英)[a)], and Xu Zhi-Zhan(徐至展)[a)]

[a)] *Key Laboratory for High Intensity Optics, Shanghai Institute of Optics and Fine Mechanics, Chinese Academy of Sciences, Shanghai* 201800, *China*

[b)] *Institute of Science and Technology for Opto-Electron Information, Yantai University, Yantai* 264005, *China*

(Received 14 May 2004; revised manuscript received 21 January 2005)

The coherent anti-Stokes Raman scattering (CARS) microscope with the combination of confocal and CARS techniques is a remarkable alternative for imaging chemical or biological specimens that neither fluoresce nor tolerate labelling. CARS is a nonlinear optical process, the imaging properties of CARS microscopy will be very different from the conventional confocal microscope. In this paper, the intensity distribution and the polarization property of the optical field near the focus was calculated. By using the Green function, the precise analytic solution to the wave equation of a Hertzian dipole source was obtained. We found that the intensity distributions vary considerably with the different experimental configurations and the different specimen shapes. So the conventional description of microscope (e.g. the point spread function) will fail to describe the imaging properties of the CARS microscope.

Keywords: microscope, coherent anti-Stokes Raman scattering, Hertzian dipole, Green function
PACC: 0760P

1. Introduction

The microscope with the combination of confocal and multiphoton fluorescence techniques has become a powerful tool for three-dimensional (3D) imaging of chemical and biological specimens, especially for live cells,[1] while various natural and artificial fluorescent probes for cellular constituents have been developed considerably. For chemical or biological specimens that neither fluoresce nor tolerate labelling, the infrared or spontaneous Raman microscope are alternatives based on the vibrational properties of molecules. The disadvantages of the conventional infrared microscope are the low spatial resolution due to the long wavelength and the strong infrared absorption of water. Submicron spatial resolution can be obtained by the Raman microscope with the confocal technique.[1] However, the intrinsic weak Raman signal needs high laser power and is often overwhelmed by the fluorescence background. So the coherent anti-Stokes Raman scattering (CARS) microscope was proposed,[1,2] and many experimental results have been achieved. In the previous experiments,[2] two excitation beams were loosely focused at an angle to satisfy the phase matching condition. The overlap region of these two beams was about 10μm in diameter and about 30μm along the optical axis. It is difficult to realize the section imaging. If the CARS excitation beams are tightly focused through a large-numerical aperture (NA) objective, 3D resolution is expected.[1] Sequentially, the polarization CARS microscope,[3] the epi-detected CARS microscope,[4] and the time-resolved CARS microscope [5] were demonstrated. In theory, Potma *et al*[6] calculated the 3D transfer function of CARS microscope by solving the wave equation with the slowly varying envelope approximation (SVEA). Cheng *et al*[7] characterized the CARS microscope by solving approximately the wave equation with the Green function.

CARS is a third-order nonlinear optical process[8] that involves a pump beam and a Stokes beam at frequencies of $\omega_{\rm p}$ and $\omega_{\rm s}$, respectively. The CARS signal at the anti-Stokes frequency of $\omega_{\rm as} = 2\omega_{\rm p} - \omega_{\rm s}$ is resonantly enhanced when $\omega_{\rm p} - \omega_{\rm s}$ is tuned to a Raman band, and the propagation direction of the CARS signals is determined by the phase-matching conditions. The diagrams of energy and phase-matching conditions are shown in Fig.1. Since CARS is a four-wave-

†E-mail: jacobyuan@yahoo.com.cn

mixing process, the nonlinear dependence of CARS intensity on the incident intensities, i.e. $I_{\mathrm{CARS}} \sim I_{\mathrm{p}}^2 I_{\mathrm{s}}$, determines that only in the focal volume the CARS can be excited. And the phase-matching conditions determine that the propagation of CARS signals will vary considerably with different CARS frequencies and different specimen shapes. The conventional description of microscope, such as point-spread function (PSF), will fail to depict the characteristics of CARS microscope.

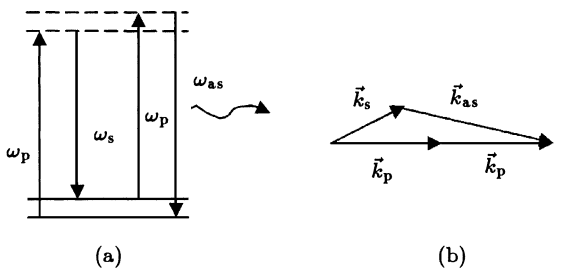


Fig.1. Diagrams of energy (a) and phase-matching (b) for CARS. (a) ω_{p}, ω_{s} and ω_{as}, are the frequencies of pump, Stokes and anti-Stokes beams respectively. (b) $\vec{k}_{\mathrm{p}}$, $\vec{k}_{\mathrm{s}}$ and $\vec{k}_{\mathrm{as}}$, are the wave vectors of pump, Stokes and anti-Stokes beams respectively.

In this paper, we calculate the focal profile and the polarization property of the focus field with the vector method.[9] Using the Green function, we obtain the precise analytic solution of the wave equation of a Hertzian dipole source, and find that the propagation of CARS signals, and the intensity distributions of CARS signals emitted by specimens with different shapes and sizes are very different.

2. Theory

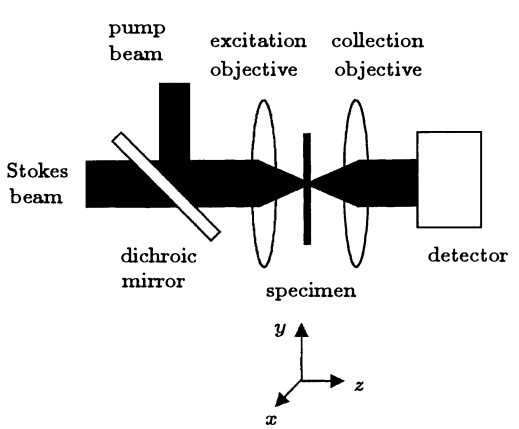


Fig.2. The experimental layout of the CARS microscopy in transmission mode.

Figure 2 is the experimental layout of the CARS microscope in transmission mode, in which the pump beam and the Stokes beam are combined collinearly by a dichroic beam splitter and focused by an excitation objective into the specimen. The CARS is detected by a photoelectric detector after collecting by a collection objective. The pump beam, Stokes beam, and CARS propagate along the z-axis.

According to the nonlinear optics principle, the excitation beams will polarize the molecules of the specimen to an electronic dipole approximatively, and the dipole moment for CARS can be expressed as follows:[8]

$$\boldsymbol{P}_{\mathrm{CARS}} = \chi^{(3)}_{\mathrm{CARS}} : \boldsymbol{E}_{\mathrm{p}} \boldsymbol{E}_{\mathrm{p}} \boldsymbol{E}^*_{\mathrm{s}}, \tag{1}$$

where $\chi^{(3)}_{\mathrm{CARS}}$, $\boldsymbol{E}_{\mathrm{p}}$ and $\boldsymbol{E}_{\mathrm{s}}$ are the third-order nonlinear susceptibility and the electric fields of the ω_{p} and ω_{s} beams at the polarized molecule respectively.

Then, the dipole acts as a source of a coherent emission field $\boldsymbol{E}(r,\omega)$. Suppose the molecule is at the origin of the coordinates and the polar direction of the molecule is along the x-axis, the electric field induced by this dipole $\boldsymbol{E}(r,\omega)$ will be[10]

$$\begin{aligned}\boldsymbol{E}(r,\omega) =& \frac{\mathrm{i}\omega\mu P_{\mathrm{CARS}}}{4\pi}\left[\frac{x^2}{k^2}\left(-\frac{k^2}{r^3}-\frac{3\mathrm{i}k}{r^4}+\frac{3}{r^5}\right)\hat{\boldsymbol{x}}\right.\\ &+\left(\frac{1}{r}+\frac{\mathrm{i}}{kr^2}-\frac{1}{k^2r^3}\right)\hat{\boldsymbol{x}}\\ &+\frac{xy}{k^2}\left(-\frac{k^2}{r^3}-\frac{3\mathrm{i}k}{r^4}+\frac{3}{r^5}\right)\hat{\boldsymbol{y}}\\ &\left.+\frac{xz}{k^2}\left(-\frac{k^2}{r^3}-\frac{3\mathrm{i}k}{r^4}+\frac{3}{r^5}\right)\hat{\boldsymbol{z}}\right],\end{aligned} \tag{2}$$

where $r = \sqrt{x^2+y^2+z^2}$, and ω, k are the frequency and wavenumber of the CARS respectively.

The distribution of the CARS electronic field at the position $Q(x,y,z)$ will be the superposition of the $\boldsymbol{E}(r,\omega)$ from all the dipoles.

According to Eq.(1), the dependence of the CARS signal intensity on the incident beam intensity is $I_{\mathrm{CARS}} \sim I_{\mathrm{p}}^2 I_{\mathrm{s}}$, hence it is reasonable to think that only in the focal region the CARS can be excited. So the intensity distribution of the incident beams near the focus will play an important role in the CARS excitation.

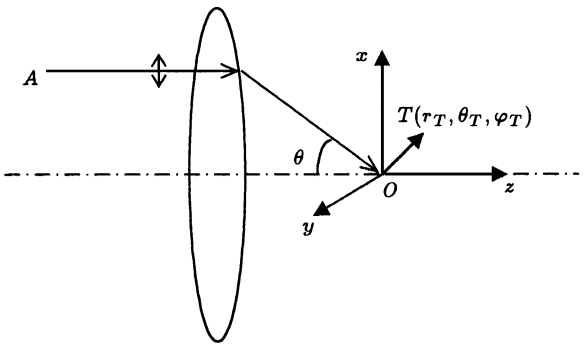


Fig.3. The field vectors near the focus of the objective for a single incident beam. The z-axis of the coordinates O-xyz is along the optical axis. The incident beams are parallel to the optical axis, and the polar direction is along the x-axis. The beams after the objective converge at the focus O, and θ is the angle between the convergent line and the optical axis. T is an arbitrary point near the focus and its spheral coordinates is (r_T, θ_T, ϕ_T).

Refer to Fig.3, where θ is the angle between the convergent beam and the optical axis, and A is the amplitude of the incident beam. Suppose the polarized direction of the incident beam is along the x axis, the components of the field vectors at a point $T(r_T, \theta_T, \phi_T)$ (the coordinates of (r_T, θ_T, ϕ_T) are shown in Fig.3) in the image space are[9]

$$\begin{cases} E_x(T) = -\mathrm{i}A(I_0 + I_2 \cos 2\phi_P), \\ E_y(T) = -\mathrm{i}AI_2 \sin 2\phi_P, \\ E_z(T) = -\mathrm{i}AI_1 \cos 2\phi_P, \end{cases} \tag{3}$$

where

$$\begin{cases} I_0 = \int_0^\alpha \cos^{\frac{1}{2}}\theta \sin\theta (1+\cos\theta) J_0(kr_T \sin\theta \sin\theta_T) \exp(\mathrm{i}kr_T \cos\theta \cos\theta_T)\,\mathrm{d}\theta, \\ I_1 = \int_0^\alpha \cos^{\frac{1}{2}}\theta \sin^2\theta J_1(kr_T \sin\theta \sin\theta_T) \exp(\mathrm{i}kr_T \cos\theta \cos\theta_T)\,\mathrm{d}\theta, \\ I_2 = \int_0^\alpha \cos^{\frac{1}{2}}\theta \sin\theta (1-\cos\theta) J_2(kr_T \sin\theta \sin\theta_T) \exp(\mathrm{i}kr_T \cos\theta \cos\theta_T)\,\mathrm{d}\theta; \end{cases} \tag{4}$$

and α is the maximum of θ.

3. Simulation

When the wavelength of the incident beam is 700nm, the numerical aperture of the objective is 1.0, and the polarized direction of the incident beam is along the x axis, we calculate the components of the field vectors near the focus as in Fig.4. Figures 4(a) and 4(b) are in the $r-\phi$ space and the $r-\theta$ space respectively, and $E = \sqrt{|E_x|^2 + |E_y|^2 + |E_z|^2}$. From Fig.4, we can see that E_y and E_z are very weak compared with E_x, and E is equal to E_x approximately.

Suppose the specimen is of isotropy and non-attenuation, all the components of the susceptibility tensor $\chi^{(3)}_{\mathrm{CARS}}$ except for the diagonal ones are zero, and the diagonal components are equal. When the wavelengths of the pump beam λ_{p} and the Stokes beam λ_{s} are 700 and 800nm respectively, we calculate the dipole moment near the focus as shown in Fig.5. Figures 5(a) and 5(b) are depicted in the $r-\phi$ and $r-\theta$ spaces respectively, and $P = \sqrt{|P_x|^2 + |P_y|^2 + |P_z|^2}$.

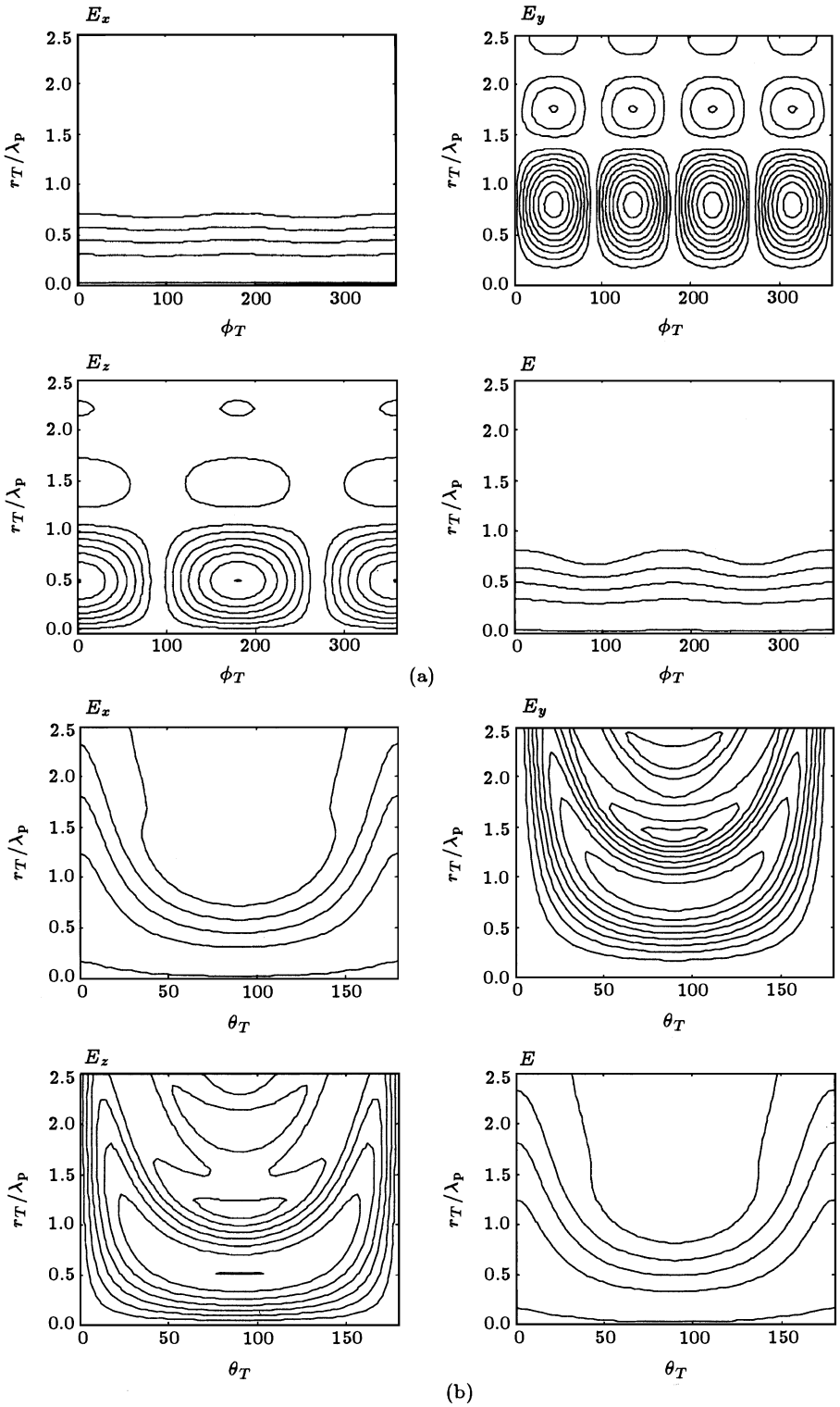


Fig.4. The contours of components of the electric field near the focus, wavelength λ=700nm, numerical aperture NA=1.0. (a) in the $r-\phi$ space, (b) in the $r-\theta$ space.

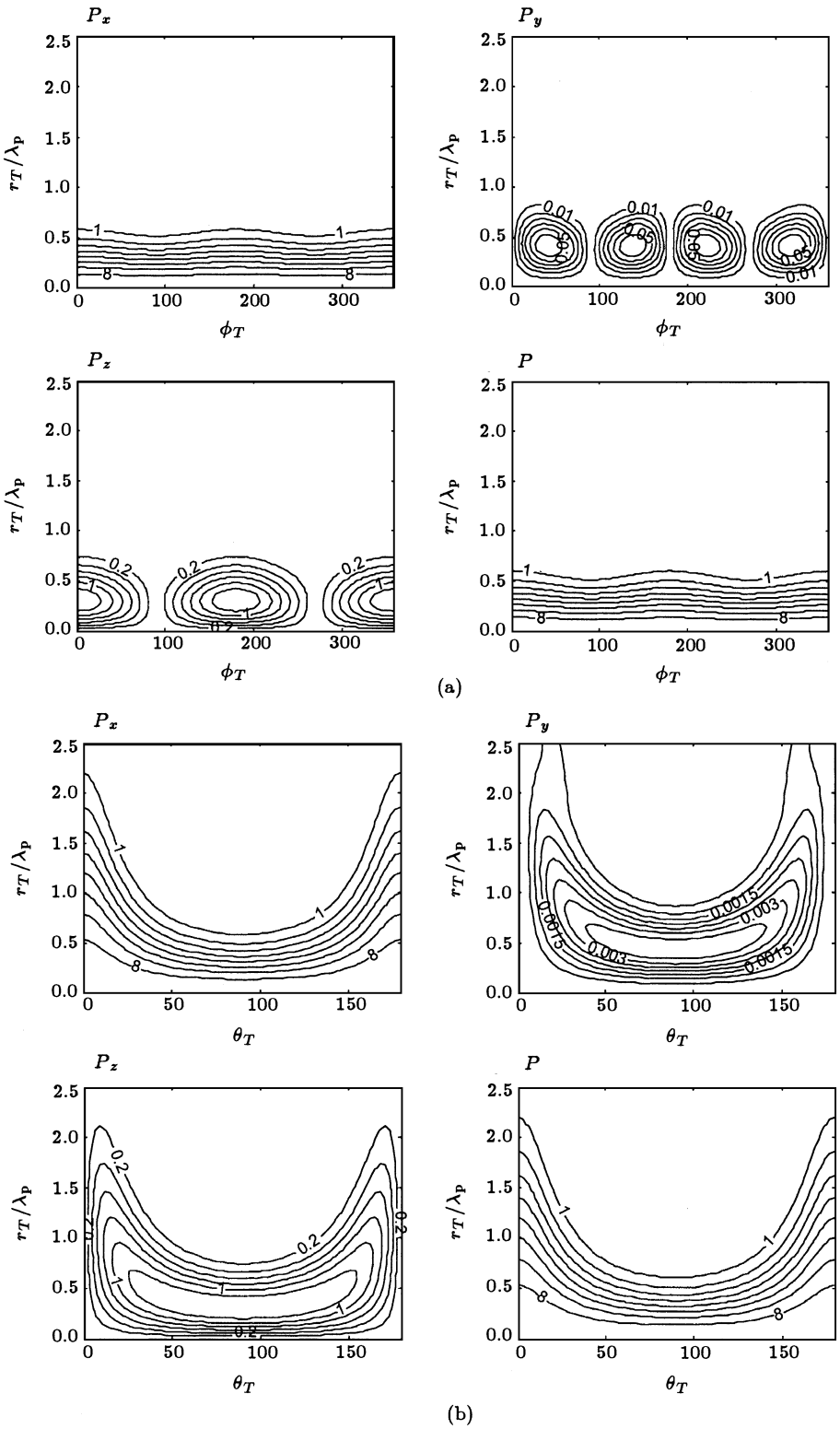


Fig.5. The contours of components of the CARS dipole moments near the focus, for wavelengths of the pump beam and the Stokes beam being 700 and 800nm, respectively.

For an isotropic medium bead whose centre is placed at the focus, when the radius is taken to be 0.1, 0.5, 1.0, and $1.5\lambda_p$, the distributions of the CARS signals are plotted in Figs.6(a)–(d) respectively. In Fig.6, each piece is a section at different z coordinates ($-1.65 \leq z \leq 1.75$, and the interval $\Delta z = 0.1\lambda_p$).

When the radius of the medium bead is $0.1\lambda_p$, the CARS signals are about the same in both the forward and backward directions. With increasing radius, the distributions of CARS become different in both directions, and the forward intensity is more and more strong compared with the backward one.

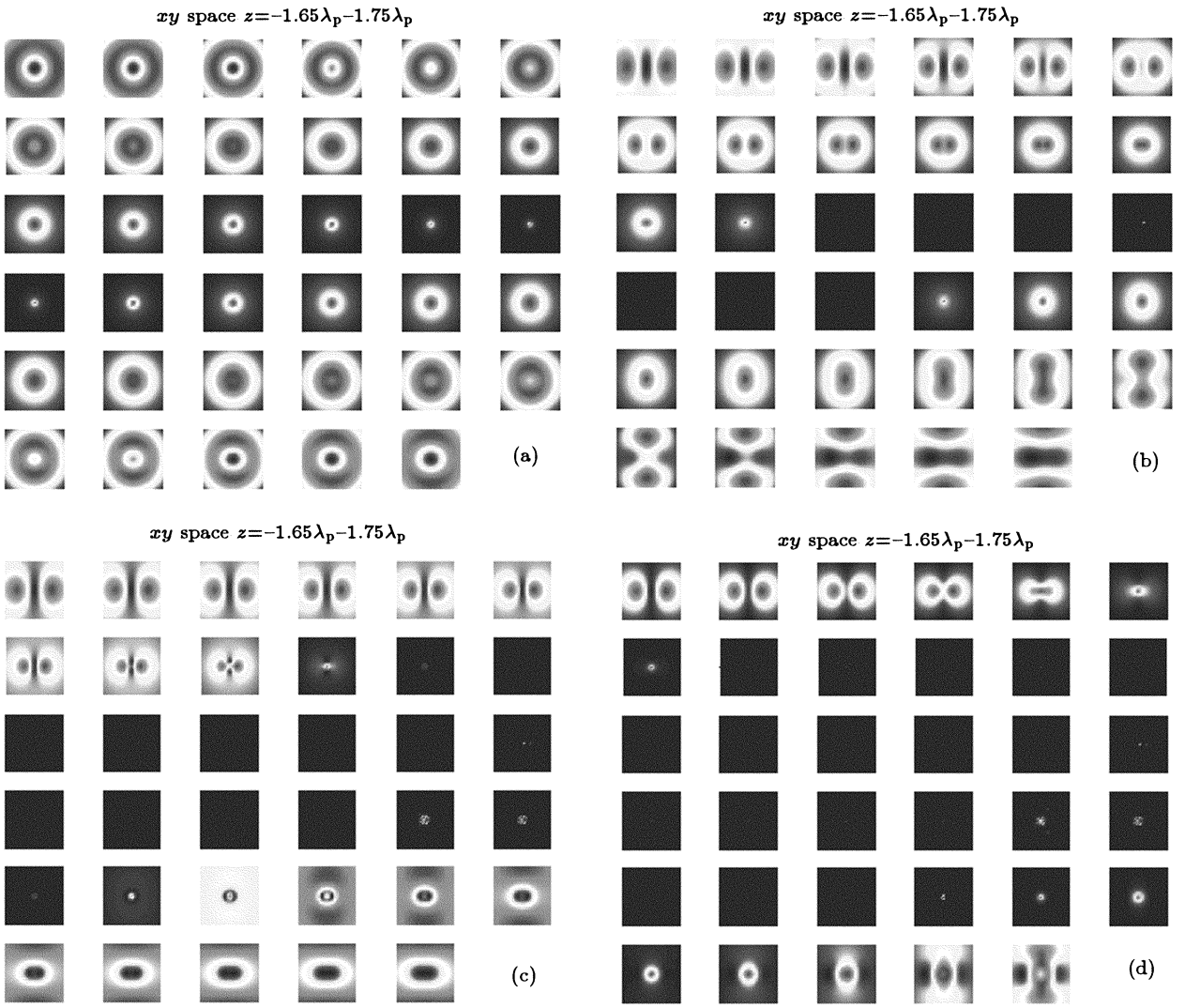


Fig.6. The distributions of the CARS signals near the focus, for an isotropic medium bead placed at the focus, with different radius. (a) r=0.1λ_p, (b) r=0.5λ_p, (c) r==1.0λ_p, (d) r=1.5λ_p.

For a disc specimen with a thickness $1.0\lambda_p$, placed at the focus with its axis along the optical axis, the CARS distributions at different z coordinates ($-1.65 \leq z \leq 1.75, \Delta z = 0.1\lambda_p$) are shown in Fig.7 (a), from which the CARS distributions are seen to be about the same in both forward and backward directions.

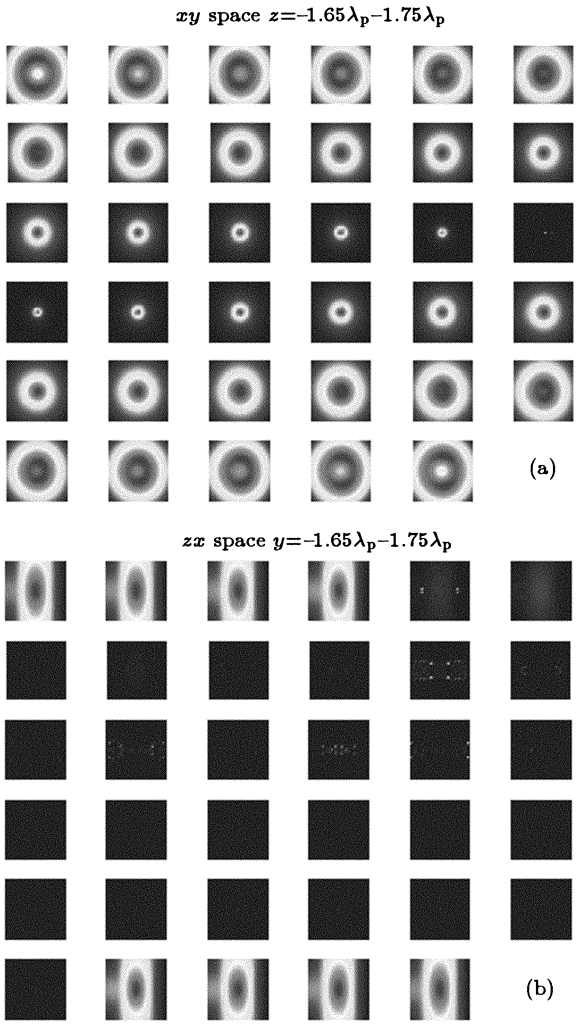


Fig.7. The CARS distributions for various specimens with different shapes at different scales. (a) a disc specimen with thickness $1.0\lambda_{\rm p}$, placed at the focus and its axis along the optical axis. The CARS distributions are about the same in both forward and backward directions. $-1.65 \leq z \leq 1.75$, $\Delta z = 0.1\lambda_{\rm p}$. (b) a rod specimen with radius $2.0\lambda_{\rm p}$, placed at the focus and its axis along the optical axis. The CARS scatters at larger angles, and their intensity in forward direction is stronger than in backward direction. $-1.65 \leq y \leq 1.75$, $\Delta y = 0.1\lambda_{\rm p}$.

For a rod specimen with a radius $2.0\lambda_{\rm p}$, placed at the focus with its axis along the optical axis, the CARS distributions at different y coordinates ($-1.65 \leq y \leq 1.75$,$\Delta y = 0.1\lambda_{\rm p}$) are shown in Fig.7(b), from which we can see that the CARS scatters at larger angles, and their intensity in the forward direction is much stronger than that in the backward direction.

4. Conclusions

CARS microscopy has complicated imaging characteristics which are very different from the conventional incoherent microscopy. In CARS microscopy, the CARS signals are affected not only by the experimental configuration, but also by the specimen size and shape. So, in our opinion, the conventional description of microscopy (such as point spread function) will fail to describe the imaging characteristics of the CARS microscope.

Our calculations give quantitative imaging characteristics of the CARS microscope for isotropic and non-attenuation specimens. From the nonlinear dependence of the CARS intensity on the incident intensity, the available excitation volume decreases considerably and the resolving power increases accordingly. To satisfy the phase-matching conditions, the objective with a large numerical aperture should be used generally. So the imaging formula based on vector diffraction theory should be used instead of the scalar theory. Because the intensity distributions of CARS signals depend on the shapes and sizes of the specimens, we can in principle estimate the shapes and sizes of the specimens by the CARS distributions.

References

[1] Zumbusch A, Holton G R and Xie X Sunney 1999 *Phys. Rev. Lett.* **82** 4142

[2] Duncan M D, Reintjes J and Manuccia T J 1982 *Opt. Lett.* **7** 350

[3] Cheng J X, Lewis D Book and Xie X Sunney 2001 *Opt. Lett.* **26** 1341

[4] Cheng J X, Volkmer A, Book L D and Xie X Sunney 2001 *Lett. to J. Phys. Chem.* B **105** 1277

[5] Volkmer A, Book L D and Xie X Sunney 2002 *Appl. Phys. Lett.* **80** 1505

[6] Potma E O, de Boeij W P and Wiersma D A 2000 *J. Opt. Soc. Am.* B **17** 1678

[7] Cheng J X, Volkmer A and Xie X Sunney 2002 *J. Opt. Soc. Am.* B **19** 1363

[8] Shen Y R 1984 *The Principles of Nonlinear Optics* (New York: Wiley) p42, p47, p267

[9] Wolf E 1959 *Proc. R. Soc.* A **253** 349

[10] Jin Au Kong 2003 *Electromagnetic Wave Theory* (Beijing: Publishing House of Electronics Industry) p292 (in Chinese)